1   **A Stochastic Collision-Attachment-Based Monte Carlo Simulation of Colloidal**

2   **Fouling: Transition from Foulant-Clean-Membrane Interaction to Foulant-**

3   **Fouled-Membrane Interaction**

4   Junxia Liu [†], Tianyi Huang [†], Ruibo Ji [†], Zhihong Wang [†], Chuyang Y. Tang *[‡], James

5   O. Leckie [§]

6

7   [†] School of Civil and Transportation Engineering, Guangdong University of Technology,

8   Guangzhou 510006, China

9   [‡] Department of Civil Engineering, The University of Hong Kong, Pokfulam, Hong

10   Kong

11   [§] Department of Civil and Environmental Engineering, Stanford University, Palo Alto,
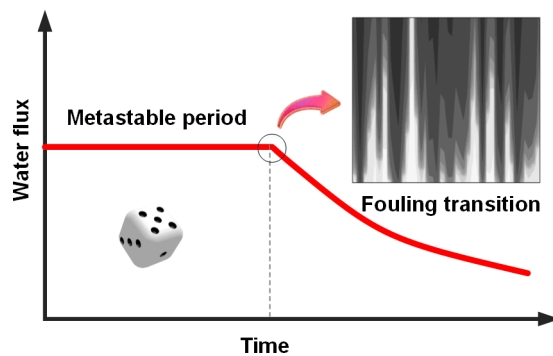
12   California, U.S.A.

13

14

15

16   *Corresponding Author:

17   Chuyang Y. Tang, tangc@hku.hk, +852 28591976

18

TABLE OF CONTENTS

2

ABSTRACT

The initial behavior of colloidal fouling is governed by foulant-clean-membrane interaction (F-M), and its long-term behavior is determined by foulant-fouled-membrane interaction (F-F). Nevertheless, the transitional fouling behavior from F-M to F-F has not been fully understood. This study reports a novel collision attachment (CA)-Monte Carlo (MC) approach, with the stochastic colloid-membrane collision events modelled by MC and the probability of colloidal attachment to the membrane determined by the interplay of flux and the energy barrier arising colloid-membrane interaction (E_m for F-M and E_f for F-F). The long-term membrane flux remains stable for large E_f, whereas severe fouling occurs when both E_m and E_f are small. Our study reveals the existence of a metastable flux behavior for the combination of large E_m but small E_f. The time evolution of flux behavior and colloidal deposition pattern shows a nearly constant flux for an extended period, with the high energy barrier E_m retarding initial colloidal deposition. However, accidental random deposition of a colloidal particle could reduce the local energy barrier (towards the smaller E_f), seeding for further colloidal deposition in its vicinity. This initiates an uneven patch-wise fouling and eventually leading to a complete transition to F-F dominated behavior. The metastable period can be effectively extended by increasing the energy barrier (E_m or E_f) or lowering flux, which provides important implications to membrane design and operation.

INTRODUCTION

Reverse osmosis (RO) and nanofiltration (NF) are widely used in desalination,[1, 2] water reuse,[3, 4] and industrial wastewater treatment.[5, 6] However, their applications are often restricted by membrane fouling. Colloidal particles, including organic macromolecules such as humic acid (HA), proteins, and polysaccharides,[7] are important foulants in RO and NF processes.[8] It has been generally agreed that colloidal fouling is governed by the interplay of hydrodynamic forces and foulant-membrane interactions.[8-10] As a notable example, Field et al. and Bacchin et al.[11-14] studied the role of permeate flux and formulated the concept of critical flux below which little fouling occurs. Solution chemistry[15-17] and membrane properties[18, 19] are equally important via their influence on foulant-membrane interactions.[20-22] For example, membrane surfaces are often designed to be more hydrophilic to impart better antifouling performance, thanks to the suppressed foulant-membrane hydrophobic attraction.[18, 19]

An interesting phenomenon in fouling is the transition from foulant-clean-membrane interaction (F-M) to foulant-fouled-membrane interaction (F-F). Although the initial fouling of a clean membrane is governed by F-M, it transits into F-F upon the complete coverage of the membrane surface by a foulant layer.[8, 23] Several experimental studies performed under constant pressure conditions reveal that the water flux could remain relatively stable for an extended period (hours to days) before the occurrence of a substantial and continued flux decline.[19, 24-27] This metastable behavior appears to be

65 more salient for a membrane with smoother and more hydrophilic surface compared to

66 other membranes with poorer antifouling properties.[27] Considering a membrane with

67 an excellent antifouling surface, it would presumably maintain a relatively stable flux

68 behavior as a result of strong F-M repulsive interaction (i.e., greater energy barrier for

69 colloidal particle attachment).[8] Nevertheless, any accidental deposition of foulant at a

70 particular location would condition the membrane surface locally, potentially shifting

71 the localized interaction into a less repulsive or even attractive F-F interaction.[10] This

72 results in a reduction in the energy barrier to initiate the propagation of fouling, in a

73 way analogous to the role of nucleation to crystallization[28, 29].

74

75 Despite its fundamental importance and practical significance with respect to

76 membrane design, process operation, and fouling control, a theoretical framework on

77 such transitional fouling behavior is yet to be established. Due to the stochastic nature

78 of this transition, deterministic models based on traditional approaches (e.g., Navier-

79 Stokes equation[30] and force balance[22]) may not work. In the current study, we report a

80 Monte Carlo (MC)-based approach to describe the random movements of colloidal

81 particles. Although MC has been successfully applied to simulate membrane pore

82 blocking,[31-33] cake formation/structure[31, 34, 35] and phase transition,[36] it has been seldom

83 used to study the F-M to F-F transitional fouling behavior. To enable the simulation of

84 the random deposition of colloidal particles on a membrane surface, we further adopt

85 the collision-attachment (CA) model,[37] in which the frequency of particle collision

86 events is simulated by the MC approach and the probability for successful particle

87 attachment for any given collision event is assessed based on the classical Boltzmann

88 distribution theory[38]. The coupled CA-MC approach is able to describe the fine details

89 of the transitional fouling behavior, underpinning the theoretical existence of

90 metastable flux and revealing its dependence on foulant-membrane interactions and

91 operational conditions. Our findings provide important guidelines and new directions

92 for fouling control.

93

94 **THEORY**

95 Membrane fouling can be idealized as a collision-attachment process: (1) colloidal

96 particles transport towards a membrane surface, leading to their collisions with the

97 surface, and (2) the attachment of the colloidal particles onto the surface.[37, 39, 40] Based

98 on the classical CA theory, the rate of colloidal particle deposition is given by the

99 product of the frequency of colloidal particle collision events and the probability of

100 successful attachment for each collision event. The CA theory has been widely adopted

101 for modelling particle-particle attachment (e.g., in the field of coagulation [41, 42]). It has

102 been recently adapted for modelling membrane fouling, recognizing a membrane

103 surface as an infinitely large and stationary particle.[37] To model the stochastic process

104 of colloidal particle transport and attachment during membrane filtration under constant

105 pressure, a two-dimensional (2D) CA-MC simulation is used in this study. Specifically,

106 the CA-MC simulation involves the following key aspects: (1) colloidal particle

107   transport in the vicinity of the membrane surface (i.e., the MC simulation of the

108   transport and collision events); (2) colloidal particle attachment based on the interplay

109   between hydrodynamic conditions and foulant-membrane interaction (i.e., the CA

110   model); and (3) the response in permeate flux as a result of membrane fouling.

111

112   Since RO membranes are not designed to treat large particles (which are removed

113   during the pre-treatment steps), this study only considers colloidal particles whose sizes

114   are << 100 nm. In this case, the diffusion of the colloidal particles are mainly caused

115   by their Brownian motion,[8, 43] while the effects of inertial lift and shear-induced

116   diffusion are negligible.[9, 44, 45]

117

118   **MC simulation of colloidal particle transport.** A feed flow channel (with length L

119   and boundary layer thickness δ) is evenly divided into n segments along its length

120   (Supporting Information S1.1). Colloidal particle transport is governed by the

121   convection in the transverse direction (caused by the crossflow velocity u in the x

122   direction), the convection towards the membrane surface (caused by the localized

123   velocity v in the $-z$ direction), and their random diffusion (Supporting Information S1.2).

124   Therefore, the displacement of the colloidal particle in horizontal direction Δx and

125   vertical direction Δz within a short time step of Δt can be obtained by:

126      $$\Delta x = u\Delta t + \sqrt{2 \times 2D\Delta t}\,\sin\theta \qquad\qquad\qquad (1a)$$

127      $$\Delta z = -v\Delta t + \sqrt{2 \times 2D\Delta t}\,\cos\theta \qquad\qquad\qquad (1b)$$

128   where D is the diffusion coefficient that can be calculated by the Stokes-Einstein

129   relationship,[46] with the term $\sqrt{2\times2D\Delta t}$ accounts for the colloidal particle diffusion in

130   a 2D plane.[47] Furthermore, the term θ is a randomly generated angle (0 - 2π) for

131   modelling of the "random walk" of the colloidal particle, which resolves the random

132   walking distance into the horizontal and vertical components ($\sqrt{2\times2D\Delta t}\sin\theta$ and

133    $\sqrt{2\times2D\Delta t}\cos\theta$, respectively). It is worthwhile to note that the vertical velocity v can

134   be estimated according to the local water flux (Supporting Information S1.3).

135

136   **CA modelling of colloidal particle attachment.** The MC simulation can be used to

137   determine the collision events. With the membrane placed at $z = 0$, a collision is

138   recognized when the value of z turns to negative (Supporting Information S1.4). The

139   probability of successful attachment can be described by the Boltzmann distribution:[37]

140    $$\frac{N_a}{N_b} = \frac{1}{\exp\left(\frac{\Delta E}{k_B T}\right)} \qquad (2)$$

141   where N_a and N_b denote the fraction of attached and unattached colloidal particles,

142   respectively, for the collision events; k_B and T are the Boltzmann's constant and the

143   absolute temperature, respectively. The term ΔE is the difference in potential energy

144   between the attached vs. non-attached states. In the context of membrane fouling, ΔE

145   is contributed by (1) the energy barrier ΔE_b arising from foulant-membrane interaction,

146   and (2) the hydrodynamic interaction caused by the drag force exerted on the colloidal

147   particle under the flux J.[37] Therefore, the probability of successful foulant attachment

148   α is given by:[37]

149 $$\alpha = \frac{N_a}{N_a + N_b} = \frac{1}{1 + \exp\left(\frac{\Delta E_b - \beta J}{k_B T}\right)} \tag{3}$$

150

151 Eq. 3 shows that colloidal particles need to overcome the energy barrier ΔE_b in order to

152 achieve a successful attachment. The value of energy barrier is given by F-M interaction

153 ($\Delta E_b = E_m$) for a clean membrane or F-F interaction ($\Delta E_b = E_f$) for a membrane

154 completely covered by foulants (also see Supporting Information S1.5 for the treatment

155 of partially fouled membranes). The value of ΔE_b is highly dependent on colloidal

156 characteristics, membrane properties as well as solution chemistry,[8] and it can be

157 determined theoretically (e.g., using DLVO or XDLVO theory [48-51]) or experimentally

158 (e.g., by interaction force measurement using atomic force microscope [21, 52-54]). A

159 greater ΔE_b resists particle deposition, i.e., leading to smaller probability of particle

160 attachment. The term βJ in Eq. 3 arises from the effect of hydrodynamics drag

161 interaction acting on the colloidal particle, where β is a proportionality coefficient that

162 is governed by the drag coefficient.[37] A larger water flux J can provide greater permeate

163 drag to overcome the energy barrier, which promotes colloidal deposition.

164

165 As a result of a collision-attachment event, a colloidal particle may disappear from the

166 feed stream and attach to the membrane surface. In this case, the deposited colloidal

167 particle will modify the local permeability of the membrane (see the section "Permeate

168 flux model") as well as change the localized energy barrier (see Supporting Information

169 S1.5). In the event of an unsuccessful attachment, the colloidal particle will remain in

170   the feed stream, in which case we assume an elastic bouncing (by resetting its new

171   vertical position as |z|, see Supporting Information S1.4).

172

173   **Permeate flux model.** The membrane water flux J can be described by:[55]

174    $$J = \frac{\Delta P}{\mu(R_m + R_f)} \tag{4}$$

175   where ΔP is the applied pressure; μ is the solution viscosity; and R_m is the hydraulic

176   resistance of the clean membrane. The foulant resistance R_f is related to the number of

177   attached colloidal particles N_f and the specific cake layer resistance α_N:

178    $$R_f = \alpha_N N_f \tag{5}$$

179

180   By combining the permeate flux model with the CA-MC approach, the stochastic

181   process of colloidal transport and attachment as well as the membrane flux behavior

182   can be modelled. The detailed simulation procedures are presented in Supporting

183   Information S1.6, with the typical simulation parameters given in Table 1.

184

Table 1. Simulation parameters

	Parameters	Value	Remarks
Particle properties	Particle size, d_p	2.0×10^{-8} m	Ref. [37]
	Particle density, ρ	1.5×10^6 g/m^3	See note[a]
	Particle mass, m_p	$\rho \pi d_p^3 / 6$	In g/#
Solution properties	Absolute temperature, T	298.15 K (25°C)	Ref. [10]
	Solution viscosity, μ	8.9×10^{-4} Pa.s	Ref. [10]
	Foulant mass concentration, C_b	5.0 g/m^3	Ref. [10]
	Particle number concentration, C_n	C_b/m_p	In #/m^3
Operation conditions	Applied pressure, ΔP	0.2-2.0 MPa	
	Crossflow velocity, u	0.2 m/s	Ref. [37]
	Membrane intrinsic resistance, R_m	4.5×10^{13} m^{-1}	Ref. [37]
	Specific cake resistance, α_N	$\alpha_f \times m_p$	See note[b]
	Water permeate flux, J	$\Delta P / (R_m + \alpha_N \times N_f)$	Eqs. 4 & 5
Diffusion	Boltzmann's constant, k_B	1.38×10^{-23} J/K	
	Diffusion coefficient, D	$k_B T / 3\pi\mu d_p$	Ref. [46]
Energy	Unit energy, $k_B T$	4.11×10^{-21} J	
	Energy barrier, ΔE_b	0-12 $k_B T$	See note[c]
	Drag energy coefficient, β	$4.19 \times 10^{-9} \times d_p$	Ref. [37]
Channel dimension	Boundary thickness, δ	5.0×10^{-6} m	Ref. [10, 37]
	Boundary length, L	5.0×10^{-5} m	
	Length of each region, L_e	1.0×10^{-6} m	
Simulation time	Time step, Δt	5.0×10^{-3} s	
	Maximum particle lifetime, t_{max}	$D \times (\exp(\delta J/D)-1)/J^2$	See Supporting Information S3

Notes:

a. The value of m_p was adopted according to the previous reports on particle density for humic acid (HA).[56]

b. α_N (in m/#) was determined via α_f (also the specific cake resistance in m/g), and in this study $\alpha_f = 3.0 \times 10^{13}$ m/g was applied according to Ref. [37]

c. The energy barrier is given by F-M interaction (E_m) for a clean membrane, F-F interaction (E_f) for a severely fouled membrane, and their hybrid during the fouling transition (see Supporting Information S1.5).

MODEL VALIDATION

In this study, we validate the CA-MC simulation by (1) comparing the particle

197 concentration polarization (CP) behavior obtained from our simulation with a

198 theoretical model,[37] and (2) comparing the simulated flux behavior with experimental

199 data.

200

201 The degree of CP at a distance of z away from the membrane surface is given by (see

202 Supporting information S2 and Ref.[37]):

203 $$\frac{C_z - \alpha C_m}{C_n - \alpha C_m} = \exp\left(\frac{J}{D}(\delta - z)\right) \qquad (6)$$

204 where C_n, C_m and C_z are the particle concentration in bulk flow, near the membrane

205 surface and at a distance z away from the membrane, respectively. Compared to the

206 classical CP model (e.g., $C_m/C_n=\exp(\delta J/D)$),[46, 57] Eq. 6 incorporates an additional term

207 αC_m to account for the loss of particles from the solution due to particle deposition on

208 the membrane (which is a depolarization mechanism often overlooked in traditional CP

209 models[46, 57-59]). Figure 1a presents the CA-MC model simulation (the discrete data

210 points) and the theoretical prediction based on Eq. 6 (the solid lines) at different values

211 of attachment coefficient ($\alpha = 0$, 0.01, 0.1 and 1). In general, the model simulation

212 agrees well with the theoretical CP lines. Specifically, severe CP occurs at $\alpha = 0$ (no

213 particle attachment, $C_m \gg C_n$). Increasing the value of α leads to less severe CP due to

214 the removal of particles from the solution phase, with a significantly reduced CP even

215 for an α of merely 0.01. At $\alpha = 1$ (every collision leads to attachment), both the CA-MC

216 simulation and the theoretical model predict negligible CP. In Figure 1a, the scattering

217 of CA-MC simulation results is due to the random Brownian motion of individual

218　colloidal particles, confirming the ability of our approach for capturing the stochastic

219　nature of particle transport and deposition.

220

221　Figure 1b further compares the simulated water flux from the CA-MC approach with

222　the experimental results for an NF membrane fouled by HA under a wide range of

223　applied pressure (50 – 300 psi). In all cases, the simulation results agree well with the

224　experimental data. The simulation also correctly predicts the greater flux decline at

225　higher applied pressure (or higher initial flux), which is in good agreement with the

226　literature.[8, 10, 27]

227
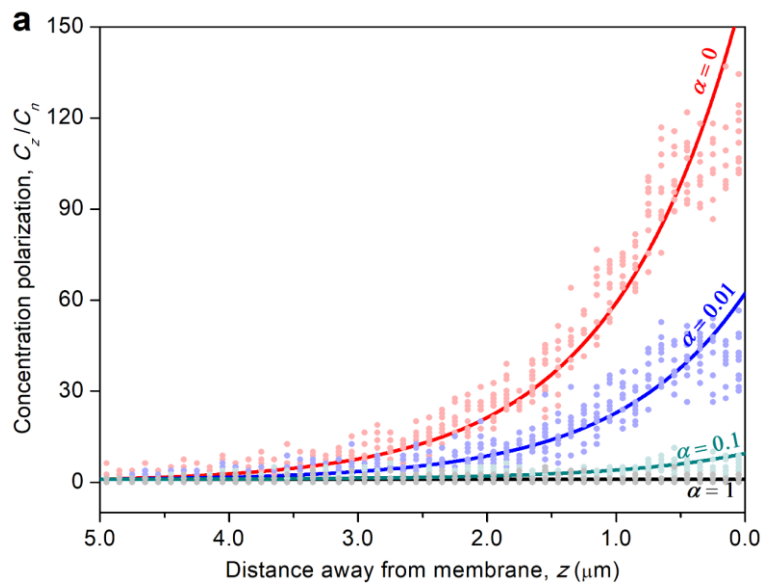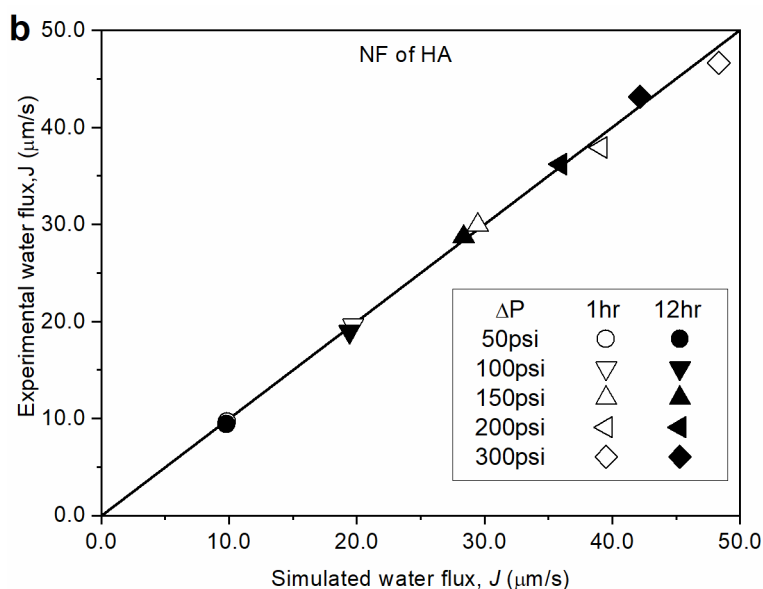
Figure 1. Model validation of (a) concentration polarization and (b) water flux decline. In part (a), the solid lines are based on Eq. 6. The scattered dots represent the simulated data based on ten runs of CA-MC simulations under a constant water flux ($J = 25\mu m/s$). In part (b), fouling of an NF membrane by humic acid is simulated under constant pressure conditions (ranging from 50 to 300 psi, corresponding to initial flux of 10-50 $\mu m/s$). The experimental data are obtained from Ref. [10], and the detailed experimental conditions are documented in our previous reports.[10, 37] Detailed simulation conditions for part (b) can be found in Supporting Information S4.

## SIMULATION RESULTS AND DISCUSSION

Flux behavior. Colloidal fouling of a clean membrane is governed by the energy barrier resulting from F-M interaction (E_m), while that of a severely fouled membrane is governed by the energy barrier resulting from F-F interaction (E_f). According to Eq. 3, a higher energy barrier can lead to a greatly reduced probability of attachment and thus slower fouling. Figure 2a shows the flux behavior at a relatively high E_f (11 k_BT) for a wide range of E_m (0-12 k_BT). With an initial flux of 20 μm/s, no obvious flux decline (<2%) occurred regardless of the value of E_m. Even for the case of $E_m = 0$ (i.e., the clean membrane presents no energy barrier against colloidal fouling), the membrane surface will be coated by the foulant to result in a highly repulsive F-F interaction that effectively slows down further foulant deposition, leading to a self-terminated fouling behavior. One example of such scenario could be the use of a negatively charged membrane for filtration of positively charged foulant. For example, Wang et al.[60] observed a relatively stable long-term flux after an initial slight flux decline for the filtration of lysozyme by a NF membrane (NF270) thanks to the more repulsive F-F interaction.
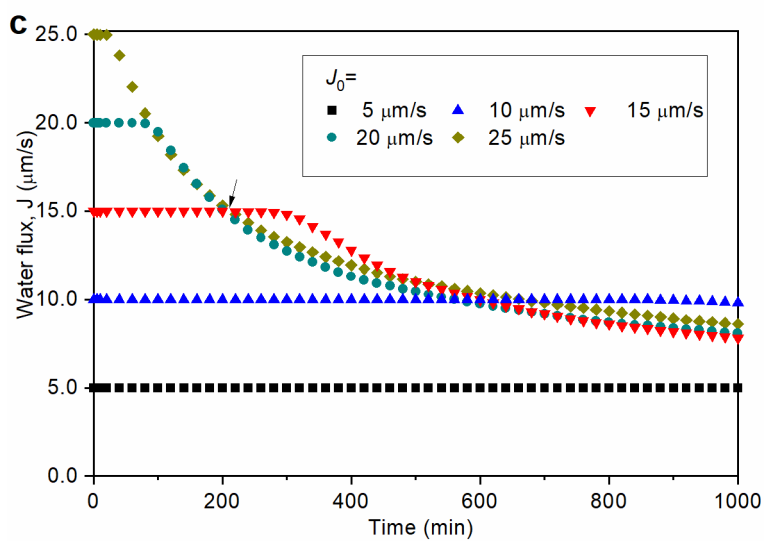
256

257

258
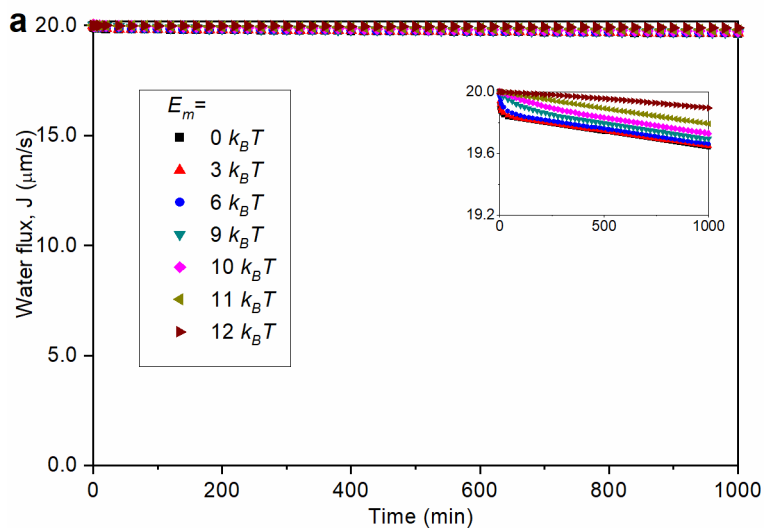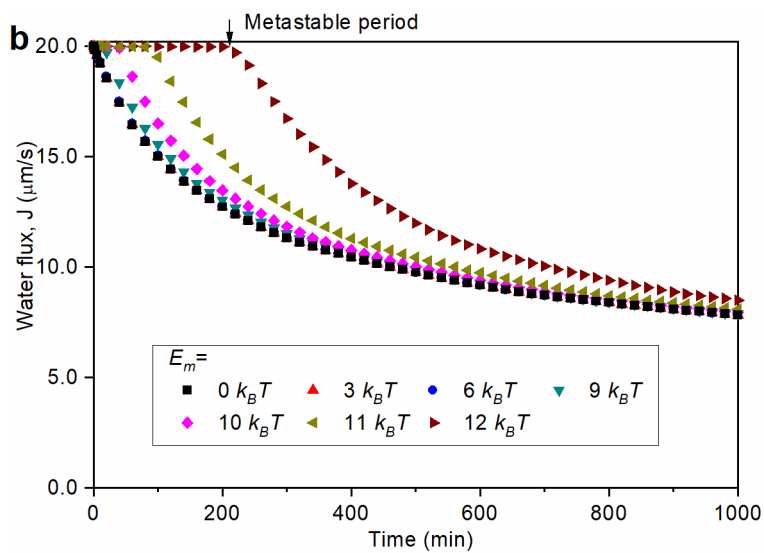
Figure 2. Effect of energy barrier and initial flux on flux behavior. (a) Effect of E_m at E_f = 11 k_BT and J_0 = 20 μm/s; (b) Effect of E_m at E_f = 3 k_BT and J_0 = 20 μm/s; (c) Effect of J_0 at E_m =11 k_BT and E_f =3 k_BT. See other simulation parameters in Table 1.

16

262

263 Much severer flux decline occurs for a lower E_f value of 3 k_BT (Figure 2b). At a long

264 filtration time of 1000 min, the decline in water flux is largely independent of E_m (0-12

265 k_BT). This result agrees well with the existing literature: the long-term fouling behavior

266 is independent of membrane surface properties once the surface is masked by foulant.[8,

267 10] Nevertheless, our simulation clearly shows that the initial fouling behavior is strongly

268 dependent on E_m, with a greater E_m favorable in retarding fouling. A metastable flux

269 behavior appears for $E_m > 9$ k_BT. For example, at $E_m = 12$ k_BT, stable flux can be

270 maintained initially before the occurrence of an obvious decline at around 220 min.

271 This metastable period decreases for smaller E_m values and becomes barely noticeable

272 with a value of 17 min at $E_m = 9$ k_BT. These results underpin the critical importance of

273 developing antifouling membranes with more repulsive F-M interaction, which

274 prevents the fouling of clean membranes by minimizing the attachment coefficient α

275 (Eq. 3). Our results are also consistent with a recent experimental study reporting stable

276 flux for a superhydrophilic NF membrane over 60 h (attributed to strong repulsive acid-

277 base F-M interaction), yet the metastable period was less than 1h for other membranes

278 with less repulsive interactions.[19] In Figure 2b, the flux decline accecelates after the

279 metastable period. This phenomenon can be explained by the conditioning of the

280 membrane surface by the deposited foulant, eventually transitioning into a F-F

281 dominated behavior.[8, 10] Consequently, fouling in the later stage becomes nearly

282 independent of membrane surface properties.[10, 22] In the current study, the metastable

283   fouling behavior resulting from the combination of high E_m and low E_f is somewhat

284   analogous to homogenous crystalization. The slow nucleation in crystalization (due to

285   the need to overcome the energy barrier for creating new surfaces) can result in

286   metastable conditions without crystal formation for supersaturated solutions.[25]

287

288   The metastable fouling behavior is also strongly dependent on the initial water flux J_0.

289   Figure 2c shows the flux behavior for various values of J_0 at fixed E_m (11 k_BT) and E_f

290   (3 k_BT). Reducing J_0 from 25 to 15 μm/s not only makes fouling less severe but also

291   greatly extends the metastable period from 30 min (at 25 μm/s) to approximately 310

292   mins (at 15 μm/s). At lower J_0 of 10 and 5 μm/s, membrane flux remains stable over

293   the entire simulation period of 1000 min. The critical importance of initial water flux

294   has been well documented in the literature: higher water flux accelerates convection of

295   colloidal particles, promotes more severe CP, and excerts greater drag effects towards

296   the membrane surface.[8, 10, 27, 37, 40, 61, 62] The current study reveals that the metastable

297   behavior is governed by the interplay between E_m and J_0, with a longer metastable

298   period obtained at greater E_m (Figure 2b) and lower J_0 (Figure 2c). According to Eq. 3,

299   a combination of large E_m and low J_0 ensures a low probility of colloidal particle

300   attachment to the clean membrane, slowing down the membrane conditioning and thus

301   extending the metastable period.

302

303   Figure 2c also shows a flux crossover behavior. For the flux curve started with the

304   highest J_0 of 25 µm/s, fouling is so rapid that it quickly transits into a F-F dominated

305   region. This flux curve crosses over with one for J_0 = 15 µm/s at around 200 min

306   (indicated by the arrow in Figure 2c). At this crossover point, the two fouling curves

307   have the same flux, but the one started with J_0 = 25 µm/s continues with a rapid rate of

308   flux decline (due to the dominance of F-F interaction with E_f = 3 k_BT) and the one with

309   J_0 = 15 µm/s remains metastable (due to the dominance of F-M interaction with E_m =

310   11 k_BT). Similar crossover also happens for J_0 = 10 µm/s at longer duration. The current

311   study reveals that the use of a higher initial flux results in an earlier transition from F-

312   M (E_m = 11 k_BT) to F-F (E_f = 3 k_BT). This transition reduces the membrane's ability to

313   resist further foulant deposition, which is responsible for the flux crossover behavior.

314   Therefore, excessively high water flux should be strictly prohibited to avoid premature

315   occurrence of F-M to F-F transition.

316

317   **Metastable Period.** To achieve a better understanding of the metastable period, we

318   analyze a wider selection of flux-interaction energy combinations. Figure 3 plots the

319   metastable period t_{mp} as a function of E_m and J_0, with the discrete data points obtained

320   from the CA-MC simulation. At each given J_0, the logarithm of the metastable period

321   (ln t_{mp}) appears to be linearly dependent on the F-M interaction energy E_m, with a

322   doubling in t_{mp} for every increase of E_m by 0.8-0.9 k_BT. Meanwhile, the metastable

323   period increases at lower J_0 (doubling in t_{mp} for every decrease of J_0 by approximately

324   3 µm/s). Although the metastable period has the strongest dependence on E_m and J_0, we

325 also found that it has a weak dependence on E_f (with a larger E_f favoring extended

326 metastable period).

327
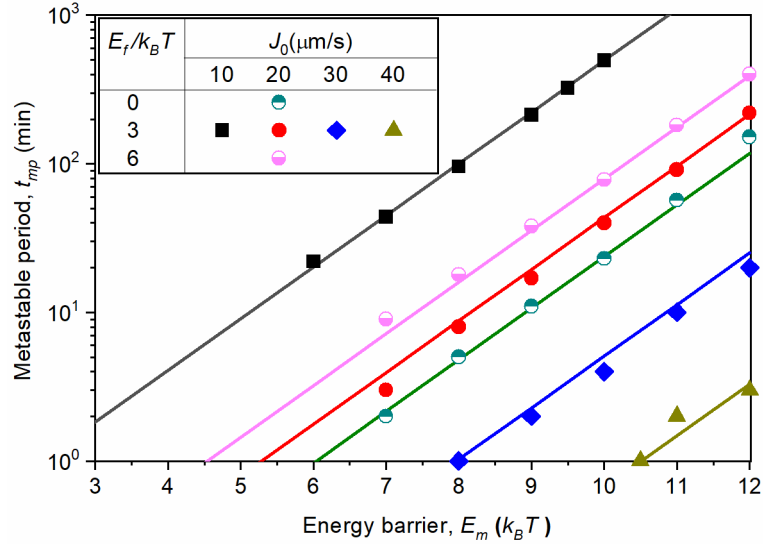
328
329 Figure 3. Effects of energy barrier and initial flux on the metastable period. A threshold
330 flux decline rate of 1‰ per minute is applied. The scattered dots represent the
331 simulation results based on the CA-MC model. Simulation conditions: E_m =6-12 k_BT,
332 E_f=0-6 k_BT, J_0=10-40 μm/s, and other conditions are shown in Table 1. The solid lines
333 are fitting lines given by $\ln t_{mp} = 0.8E_m/k_BT + 0.2E_f/k_BT - 0.174J_0 - \ln(0.00159J_0) - 4.79$,
334 with t_{mp} in min and J_0 in μm/s (R^2=0.9945). The theoretical basis of the fitting lines is
335 provided in Supporting Information S5.

336

337 **Transitional fouling behavior.** The CA-MC simulation is capable of resolving the

338 fine details of transitional fouling behavior. Figure 4a-d presents the evolution of the

339 foulant distribution pattern over time for different combinations of E_m and E_f at a fixed

340 J_0 of 20 μm/s, with the color scale representing the area number density of deposited

341 colloidal particles (i.e., the number of particles deposited in each simulation grid with

342 an area of 0.1 μm² in the current study). As expected, the combination of high E_m (11

343 k_BT) and high E_f (11 k_BT) results in very slow particle accumulation (Figure 4a), thanks

344 to the strongly repulsive F-M and F-F interactions. It takes approximately 400 min to

345 reach an average density of 100 perticles per grid (#/grid), and the number is only about

346 250 #/grid over the entire 1000-min simulation (Figure 4e). Lowering E_m to 3 k_BT while

347 keeping E_f at 11 k_BT leads to an accelerated initial particle deposition (Figure 4b),

348 reaching 100 #/grid in approximately 2 min owing to the weaker F-M repulsion.

349 Nevertheless, the subsequent deposition of colloidal particles becomes much slower

350 (slightly over 400 #/grid) at 1000 min, Figure 4e), as a result of the rapid conditioning

351 of the membrane surface by the deposited foulant and the transition to a more repulsive

352 F-F interaction. The current study reveals that a high E_f ensures long-term stable

353 membrane operation regardless of the value of E_m (Figure 2a and Figure 4a,b),

354 underpinning the critical importance of pretreatment and adjustment of water

355 chemistry[22, 60, 63, 64] for practical membrane operations. In contrast, the combination of

356 low E_m (3 k_BT) and low E_f (3 k_BT) results in almost instaneous particle deposition as

357 well as severe long-term fouling (Figure 4d), reaching approximately 100 #/grid in the

358 first min and 37,000 #/grid by the end of the 1000-min simulation (Figure 4e).

359

360 The combination of high E_m (11 k_BT) and low E_f (3 k_BT) presents an interesting scenario

361 (Figure 4c). Owing to the highly repulsive F-M interaction, the initial particle

362 deposition is rather slow (Figure 4e), in good accordance with its initial metastable

363 water flux (Figure 2b). However, a sharp transition occurs during 90 - 200 min (Figure

364 4e), accompanied with greatly accelerated particle deposition with the transition of

365 strongly repulsive F-M to an unfavorable F-F interaction. Indeed, its initial particle

366 deposition behavior is nearly identical to that for the case of $E_m = 11$ k_BT and $E_f = 11$

367 k_BT (indicating a F-M dominated behavior), while the long term behavior is nearly

368 identical to that for the case of $E_m = 3$ k_BT and $E_f = 3$ k_BT (suggesting a F-F dominated

369 behavior). In addition, the transitional window of 90 - 200 min in Figure 4e also agrees

370 well with the ending of the metastable period (90 min) for the corresponding flux curve

371 in Figure 2b.

372

373 A closer examination of the foulant distribution pattern in Figure 4c reveals that it is

374 highly non-uniform (particularly during the transitional period) compared to other cases

375 (Figure 4a, b, d). This difference is also reflected by the larger standard deviation in

376 Figure 4e (represented by the shading) for the combination of high E_m and low E_f (see

377 further discussion in Supporting Information S7). During membrane filtration, colloidal

378 particles are transported towards the membrane surface under the permeate drag, which

379 is resisted by the energy barrier[8]. While the clean membrane with $E_m = 11$ k_BT is highly

380 antifouling, an accidental deposition of foulant particle would modify the localized

381 surface properties. For the case of $E_f \ll E_m$, it leads to reduced energy barrier locally,

382 which serves as a seed to promote further particle deposition in the vicinity of the

383 existing foulant. Consequently, a patch-like "colonization" behavior is expected, where

384 the fouled patches serve as hot spots to accelerate further particle deposition (also see

385 Supporting Information S6). It is worthwhile to note that the time and location for the

22

386   occurrence of the patches are highly random due to the stochastic nature of particle

387   transport and attachment. However, each patch will grow laterally over time to expand

388   their coverage over the membrane surface, leading to an eventual complete coverage of

389   the entire membrane. Upon this completion of the F-M to F-F transition, the energy

390   barrier becomes entirely governed by E_f, rendering the later stage of fouling more

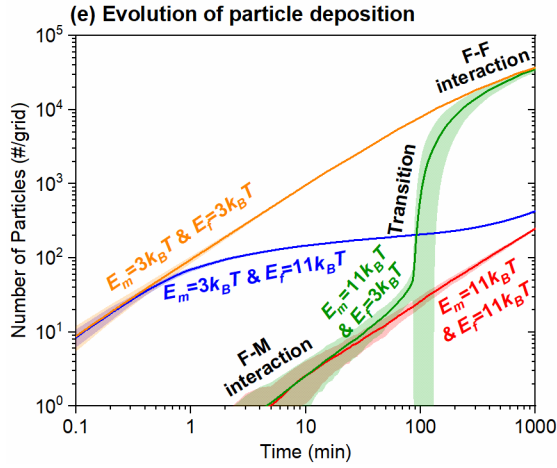391   uniform (Figure 4c and Figure 4e).

392

393

394

(e) Evolution of particle deposition
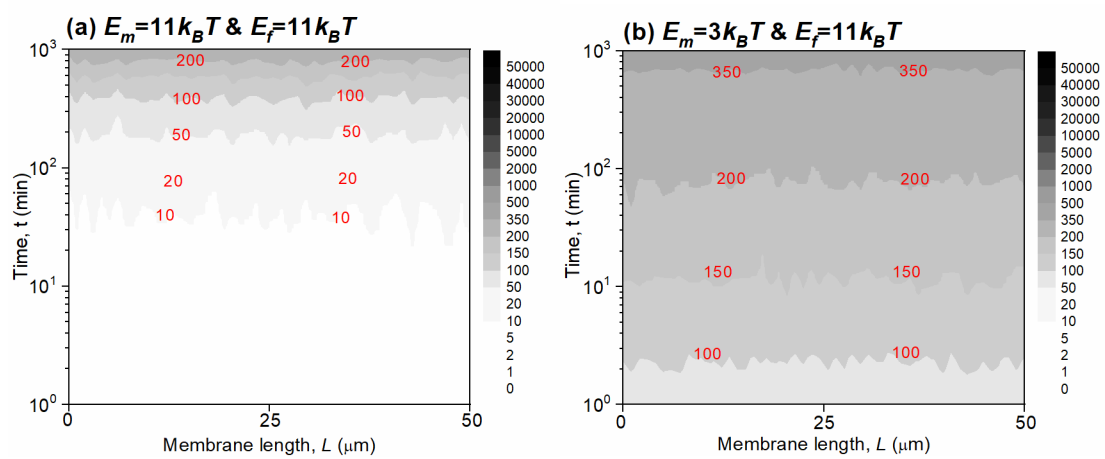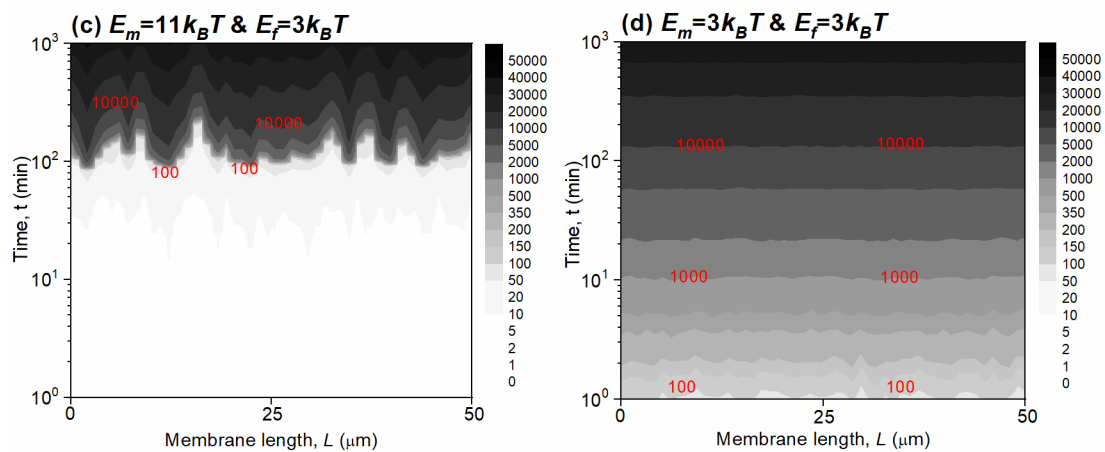
Figure 4. The role of energy barrier on the evolution of particle deposition. Parts (a-d) presents the particle deposition pattern over time for (a) $E_m = 11\ k_BT$ and $E_f = 11\ k_BT$; (b) $E_m = 3\ k_BT$ and $E_f = 11\ k_BT$; (c) $E_m = 11\ k_BT$ and $E_f = 3\ k_BT$; (d) $E_m = 3\ k_BT$ and $E_f = 3\ k_BT$. The color scale represents the area number density of deposited particles in number of particles per simulation grid (i.e., the number of particles deposited in each membrane segment with $0.1 \mu m^2$ in area). An initial flux J_0 of $20 \mu m/s$ is used in the simulation, and other simulation parameters are given in Table 1. Part (e) presents the average area number density as a function of time for different combinations of E_m and E_f values. The solid lines represent the average values. The corresponding shadings represent the standard deviations, which can be used to characterize the uniformity of foulant deposition. For the case of $E_m = 11\ k_BT$ and $E_f = 3\ k_BT$, the deposition is so non-uniform during the transition such that some regions are heavily covered by colloidal particles while other regions are nearly free of particles. Accordingly, the coefficient of variation (i.e., the ratio of standard deviation over the average value, also see Supporting Information S7) for the spatial distribution of particle deposition can be greater than 1, causing the shading of the curve to cross the horizontal axis.

To further resolve the transitional fouling behavior, Figure 5 presents the evolution of

particle accumulation, energy barrier, and attachment coefficient over time at different

initial flux values for the case of high E_m (11 k_BT) and low E_f (3 k_BT). At J_0 of 10 μm/s,

particle deposition is very slow and the membrane remains largely clean with the

exception of a few minor foulant patches towards the end of the 1000-min filtration

period. This is in good agreement with its extended metastable period (Figure 2c).

Increasing J_0 to 15 μm/s results in accelerated particle deposition, which is

24

420 accompanied with a drop of energy barrier from 11 k_BT (resulting from E_m) to 3 k_BT

421 (resulting from E_f) and a corresponding shift in the attachment coefficient. Indeed, the

422 shape of these patterns largely mirror each other. Further increase in J_0 results in an

423 earlier occurrence of transitional behavior in particle deposition, energy barrier, and

424 attachment coefficient (Figure 5), in good agreement with their shorter metastable

425 period (Figure 2c).

426
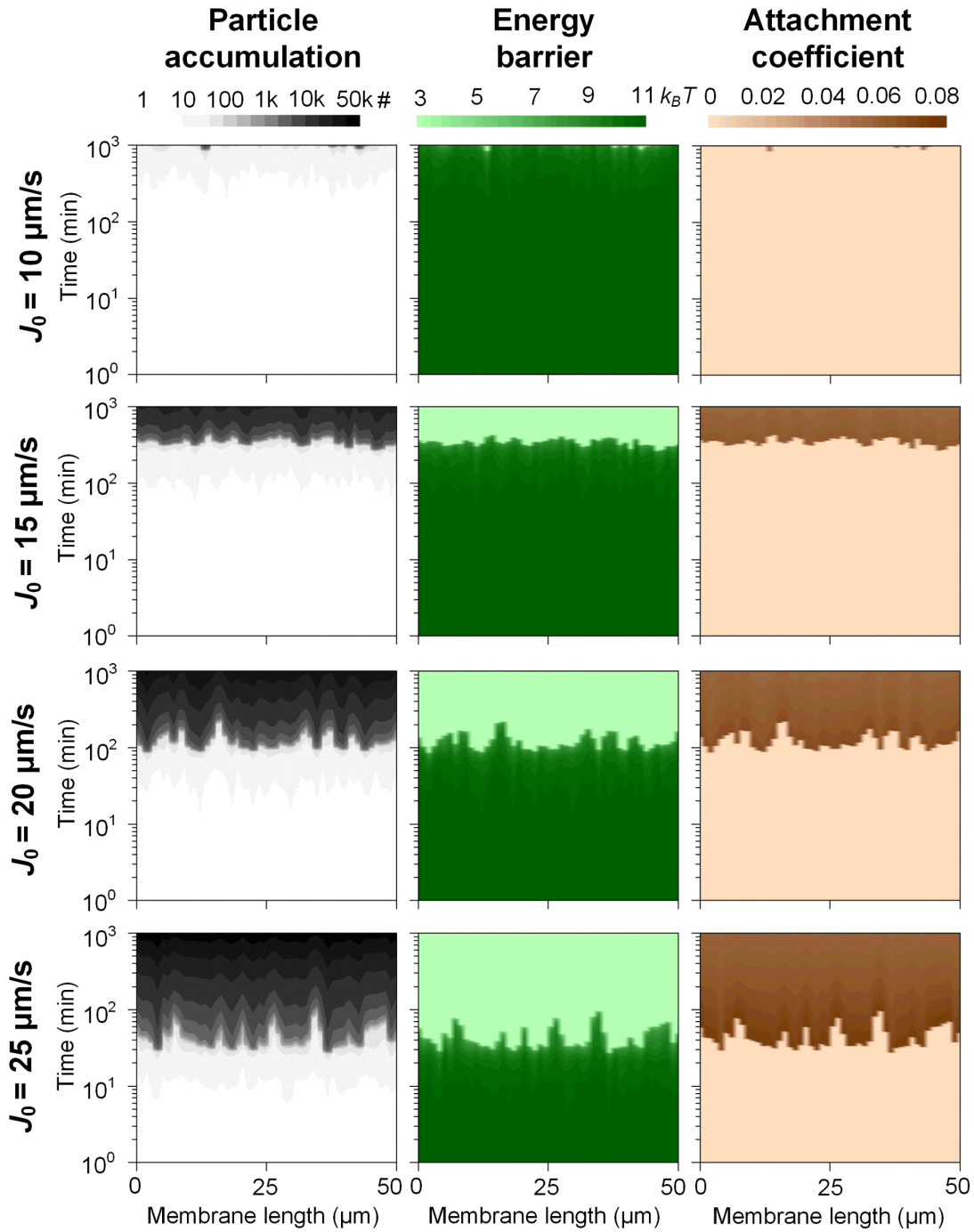
Figure 5. Evolution of particle accumulation, energy barrier, and attachment coefficient over time at different initial flux values. Simulation conditions: $E_m = 11$ k_BT and $E_f = 3$ k_BT; other parameters given in Table 1.

Implications. For the first time, the current study systematically resolves the F-M to

F-F transitional behavior during colloidal fouling using a novel CA-MC approach that

434   captures the stochastic transport and attachment of foulant particles. Our simulation

435   provides the theoretical basis for the metastable flux behavior under the condition of

436   high E_m and low E_f, with the metastable period greatly extended at increased energy

437   barrier (E_m and E_f) and lower flux. This study provides critical implications for

438   membrane design and process operation. In view of the great impact of water chemistry

439   on both F-M and F-F, pretreatment of problematic feed water provides effective

440   protection to RO and NF membranes. Although a large E_f can effectively minimize

441   fouling, its value is often constrained by the characteristics of the feed water (e.g.,

442   foulant type and properties). For applications prevailed with unfavorable E_f values, the

443   development of membranes with high E_m values is essential to achieve antifouling and

444   to maintain a stable operation over extended periods.[19] Nevertheless, it is important to

445   realize that even the best antifouling membrane may fail when it is subjected to

446   excessive flux (Figure 2c), due to the premature transition from F-M to F-F. Therefore,

447   operating below the threshold flux[10, 11, 13, 37] is critical to prevent such premature

448   membrane failures. In practice, moderate flux is often applied (e.g., 12-17 $Lm^{-2}h^{-1}$ for

449   seawater desalination and 12-45 $Lm^{-2}h^{-1}$ for bracksih water treatment).[2] The

450   combination of moderate flux and large E_m is of great practical significance to extend

451   the metastable period and thus to minimize the required cleaning frequency (e.g., into

452   months or even years).

453

454   Our study also reveals the critical role of initial foulant "colonization" in the

455 modification of the localized energy barrier (Figure 5). Therefore, upon the initial

456 occurance of foulant patches, timely cleaning is critical to prevent severe propogation

457 of further particle deposition and to restore the unfavorable F-F interaction to the more

458 repulsive F-M interaction. While existing membrane cleaning studies generally focus

459 on cleaning chemistries and choices of methods (e.g., air scouring, backflushing, and

460 chemical cleaning[63, 65, 66]), future studies also need to emphasize the timing of cleaning

461 in relation to the metastable fouling behavior and the onset of the F-M to F-F transition.

462 Our study also implies the critical importance of early fouling detection for effective

463 management of membrane operation and cleaning.

464

465 **ASSOCIATED CONTENT**

466 **Supporting Information**

467 The Supporting Information is available free of charge on the ACS Publications website.

468 S1. CA-MC model; S2. Concentration polarization model; S3. Derivation of maximum

469 particle lifetime; S4. Parameters used for model validation; S5. Derivation of

470 metastable period; S6. Colloidal particle deposition during fouling transition; S7.

471 Uniformity of colloidal particle deposition; S8. Role of cake compressibility on fouling;

472 S9. MATLAB code for the CA-MC simulation.

473

474 **AUTHOR INFORMATION**

475 **Corresponding Authors**

476 *E-mail: tangc@hku.hk. Phone: +852 28591976.

477 **ORCID**

478 Junxia Liu: 0000-0002-5856-3856

479 Chuyang Y. Tang: 0000-0002-7932-6462

480 **Notes**

481 The authors declare no competing financial interest.

ACKNOWLEDGEMENTS

486

REFERENCES

488 1. Elimelech, M.; Phillip, W. A., The Future of Seawater Desalination: Energy,
489 Technology, and the Environment. *Science* **2011,** *333*, (6043), 712-717.
490 2. Greenlee, L. F.; Lawler, D. F.; Freeman, B. D.; Marrot, B.; Moulin, P., Reverse
491 osmosis desalination: water sources, technology, and today's challenges. *Water Res.*
492 **2009,** *43*, (9), 2317-2348.
493 3. Shannon, M. A.; Bohn, P. W.; Elimelech, M.; Georgiadis, J. G.; Mariñas, B. J.;
494 Mayes, A. M., Science and technology for water purification in the coming decades.
495 *Nature* **2008,** *452*, (7185), 301-10.
496 4. Tang, C. Y.; Yang, Z.; Guo, H.; Wen, J. J.; Nghiem, L. D.; Cornelissen, E., Potable
497 Water Reuse through Advanced Membrane Technology. *Environ. Sci. Technol.* **2018,**
498 *52*, (18), 10215-10223.
499 5. Mondal, S.; Wickramasinghe, S. R., Produced water treatment by nanofiltration
500 and reverse osmosis membranes. *J. Membr. Sci.* **2008,** *322*, (1), 162-170.
501 6. Xiao, Y.; Guo, D.; Li, T.; Zhou, Q.; Shen, L.; Li, R.; Xu, Y.; Lin, H., Facile
502 fabrication of superhydrophilic nanofiltration membranes via tannic acid and irons
503 layer-by-layer self-assembly for dye separation. *Appl. Surf. Sci.* **2020,** *515*, 146063.
504 7. Buffle, J.; Wilkinson, K. J.; Stoll, S.; Filella, M.; Zhang, J. W., A generalized
505 description of aquatic colloidal interactions: The three-colloidal component approach.
506 *Environ. Sci. Technol.* **1998,** *32*, (19), 2887-2899.

507 8. Tang, C. Y.; Chong, T. H.; Fane, A. G., Colloidal interactions and fouling of NF
508 and RO membranes: A review. *Adv. Colloid Interface Sci.* **2011,** *164*, (1-2), 126-143.
509 9. Bacchin, P.; Aimar, P.; Field, R. W., Critical and sustainable fluxes: Theory,
510 experiments and applications. *J. Membr. Sci.* **2006,** *281*, (1-2), 42-69.
511 10. Tang, C. Y.; Leckie, J. O., Membrane independent limiting flux for RO and NF
512 membranes fouled by humic acid. *Environ. Sci. Technol.* **2007,** *41*, (13), 4767-73.
513 11. Field, R.; Wu, D.; Howell, J.; Gupta, B., Critical flux concept for microfiltration
514 fouling. *J. Membr. Sci.* **1995,** *100*, (3), 259-272.
515 12. Wu, D. X.; Howell, J. A.; Field, R. W., Critical flux measurement for model
516 colloids. *J. Membr. Sci.* **1999,** *152*, (1), 89-98.
517 13. Bacchin, P.; Aimar, P.; Sanchez, V., Model for colloidal fouling of membranes.
518 *AlChE J.* **1995,** *41*, (2), 368-376.
519 14. Fradin, B.; Field, R. W., Crossflow microfiltration of magnesium hydroxide
520 suspensions: determination of critical fluxes, measurement and modelling of fouling.
521 *Sep. Purif. Technol.* **1999,** *16*, (1), 25-45.
522 15. Yu, W.; Liu, T.; Crawshaw, J.; Liu, T.; Graham, N., Ultrafiltration and nanofiltration
523 membrane fouling by natural organic matter: Mechanisms and mitigation by pre-
524 ozonation and pH. *Water Res.* **2018,** *139*, 353-362.
525 16. Zhu, X.; Elimelech, M., Colloidal Fouling of Reverse Osmosis Membranes:
526 Measurements and Fouling Mechanisms. *Environ. Sci. Technol.* **1997,** *31*, (12), 3654-
527 3662.
528 17. Tang, C. Y.; Kwon, Y.-N.; Leckie, J. O., Characterization of humic acid fouled
529 reverse osmosis and nanofiltration membranes by transmission electron microscopy
530 and streaming potential measurements. *Environ. Sci. Technol.* **2007,** *41*, (3), 942-949.
531 18. Tang, C. Y.; Kwon, Y.-N.; Leckie, J. O., Probing the nano- and micro-scales of
532 reverse osmosis membranes - A comprehensive characterization of physiochemical
533 properties of uncoated and coated membranes by XPS, TEM, ATR-FTIR, and streaming
534 potential measurements. *J. Membr. Sci.* **2007,** *287*, (1), 146-156.
535 19. Shan, L.; Fan, H.; Guo, H.; Ji, S.; Zhang, G., Natural organic matter fouling
536 behaviors on superwetting nanofiltration membranes. *Water Res.* **2016,** *93*, 121-132.
537 20. Lee, S.; Elimelech, M., Relating organic fouling of reverse osmosis membranes to
538 intermolecular adhesion forces. *Environ. Sci. Technol.* **2006,** *40*, (3), 980-987.
539 21. Li, Q. L.; Elimelech, M., Organic fouling and chemical cleaning of nanofiltration
540 membranes: Measurements and mechanisms. *Environ. Sci. Technol.* **2004,** *38*, (17),
541 4683-4693.
542 22. Tang, C. Y.; Kwon, Y. N.; Leckie, J. O., The role of foulant–foulant electrostatic
543 interaction on limiting flux for RO and NF membranes during humic acid fouling—
544 Theoretical basis, experimental evidence, and AFM interaction force measurement. *J.*
545 *Membr. Sci.* **2009,** *326*, (2), 526-532.
546 23. Wang, L.; Miao, R.; Wang, X.; Lv, Y.; Meng, X.; Yang, Y.; Huang, D.; Feng, L.;
547 Liu, Z.; Ju, K., Fouling Behavior of Typical Organic Foulants in Polyvinylidene
548 Fluoride Ultrafiltration Membranes: Characterization from Microforces. *Environ. Sci.*

549 *Technol.* **2013,** *47*, (8), 3708-3714.

550 24. Li, Q.; Xu, Z.; Pinnau, I., Fouling of reverse osmosis membranes by biopolymers

551 in wastewater secondary effluent: Role of membrane surface properties and initial

552 permeate flux. *J. Membr. Sci.* **2007,** *290*, (1), 173-181.

553 25. Wang, J.; Wang, L.; Miao, R.; Lv, Y.; Wang, X.; Meng, X.; Yang, R.; Zhang, X.,

554 Enhanced gypsum scaling by organic fouling layer on nanofiltration membrane:

555 Characteristics and mechanisms. *Water Res.* **2016,** *91*, 203-213.

556 26. Wang, K.; Xu, L.; Li, K.; Liu, L.; Zhang, Y.; Wang, J., Development of polyaniline

557 conductive membrane for electrically enhanced membrane fouling mitigation. *J.*

558 *Membr. Sci.* **2019,** *570-571*, 371-379.

559 27. Wang, Y.-N.; Tang, C. Y., Protein fouling of nanofiltration, reverse osmosis, and

560 ultrafiltration membranes-The role of hydrodynamic conditions, solution chemistry,

561 and membrane properties. *J. Membr. Sci.* **2011,** *376*, (1-2), 275-282.

562 28. Le Gouellec, Y. A.; Elimelech, M., Calcium sulfate (gypsum) scaling in

563 nanofiltration of agricultural drainage water. *J. Membr. Sci.* **2002,** *205*, (1-2), 279-291.

564 29. Lin, C. J.; Shirazi, S.; Rao, P., Mechanistic model for CaSO4 fouling on

565 nanofiltration membrane. *J. Environ. Eng.* **2005,** *131*, (10), 1387-1392.

566 30. Amokrane, M.; Sadaoui, D.; Koutsou, C.; Karabelas, A.; Dudeck, M., A study of

567 flow field and concentration polarization evolution in membrane channels with two-

568 dimensional spacers during water desalination. *J. Membr. Sci.* **2015,** *477*, 139-150.

569 31. Chen, Y.; Kim, H., Monte Carlo simulation of pore blocking and cake formation

570 by interfacial interactions during membrane filtration. *Desalination* **2008,** *233*, (1), 258-

571 266.

572 32. Chen, Y.; Hu, X.; Kim, H., Monte Carlo simulation of pore blocking phenomena in

573 cross-flow microfiltration. *Water Res.* **2011,** *45*, (20), 6789-6797.

574 33. Kawakatsu, T.; Nakajima, M.; Nakao, S. I.; Kimura, S., Three-dimensional

575 simulation of random packing and pore blocking phenomena during microfiltration.

576 *Desalination* **1995,** *101*, (3), 203-209.

577 34. Kim, A. S.; Hoek, E. M. V., Cake structure in dead-end membrane filtration: Monte

578 Carlo simulations. *Environ. Eng. Sci.* **2002,** *19*, (6), 373-386.

579 35. Lin, C. L.; Miller, J. D., Pore structure and network analysis of filter cake. *Chem.*

580 *Eng. J.* **2000,** *80*, (1–3), 221-231.

581 36. Chen, J. C.; Elimelech, M.; Kim, A. S., Monte Carlo simulation of colloidal

582 membrane filtration: Model development with application to characterization of colloid

583 phase transition. *J. Membr. Sci.* **2005,** *255*, (1), 291-305.

584 37. Liu, J.; Wang, Z.; Tang, C. Y.; Leckie, J. O., Modeling Dynamics of Colloidal

585 Fouling of RO/NF Membranes with A Novel Collision-Attachment Approach. *Environ.*

586 *Sci. Technol.* **2018,** *52*, (3), 1471-1478.

587 38. Landau, L. D.; Lifshitz, E. M., CHAPTER IV - IDEAL GASES. In *Statistical*

588 *Physics (Third Edition)*, Landau, L. D.; Lifshitz, E. M., Eds. Butterworth-Heinemann:

589 Oxford, 1980; pp 111-157.

590 39. Henry, C.; Minier, J. P.; Lefèvre, G., Towards a description of particulate fouling:

from single particle deposition to clogging. *Adv. Colloid Interface Sci.* **2012,** *185-186*, (12), 34-76.

40. She, Q. H.; Tang, C. Y.; Wang, Y. N.; Zhang, Z. J., The role of hydrodynamic conditions and solution chemistry on protein fouling during ultrafiltration. *Desalination* **2009,** *249*, (3), 1079-1087.

41. Valioulis, I. A.; List, E. J., Collision efficiencies of diffusing spherical particles: hydrodynamic, van der Waals and electrostatic forces. *Adv. Colloid Interface Sci.* **1984,** *20*, (1), 1-20.

42. Thomas, D.; Judd, S.; Fawcett, N., Flocculation modelling: a review. *Water Res.* **1999,** *33*, (7), 1579-1592.

43. Herterich, J. G.; Griffiths, I. M.; Vella, D.; Field, R. W., The effect of a concentration-dependent viscosity on particle transport in a channel flow with porous walls. *AIChE J.* **2014,** *60*, (5), 1891-1904.

44. Zhang, G.; Zhang, J.; Wang, L.; Meng, Q.; Wang, J., Fouling mechanism of low-pressure hollow fiber membranes used in separating nanosized photocatalysts. *J. Membr. Sci.* **2012,** *389*, 532-543.

45. Kim, M.-m.; Zydney, A. L., Theoretical analysis of particle trajectories and sieving in a two-dimensional cross-flow filtration system. *J. Membr. Sci.* **2006,** *281*, (1-2), 666-675.

46. Porter, M. C., Concentration Polarization with Membrane Ultrafiltration. *Ind Eng Chem Prod Res Dev* **1972,** *11*, (3), 234-248.

47. Krapf, D., Chapter Five - Mechanisms Underlying Anomalous Diffusion in the Plasma Membrane. In *Curr. Top. Membr.*, Kenworthy, A. K., Ed. Academic Press: 2015; Vol. 75, pp 167-207.

48. Weroński, P.; Elimelech, M., Novel numerical method for calculating initial flux of colloid particle adsorption through an energy barrier. *J. Colloid Interface Sci.* **2008,** *319*, (2), 406-415.

49. Hoek, E. M.; Bhattacharjee, S.; Elimelech, M., Effect of membrane surface roughness on colloid− membrane DLVO interactions. *Langmuir* **2003,** *19*, (11), 4836-4847.

50. Jarusutthirak, C.; Amy, G., Role of soluble microbial products (SMP) in membrane fouling and flux decline. *Environ. Sci. Technol.* **2006,** *40*, (3), 969-974.

51. Chen, J.; Shen, L.; Zhang, M.; Hong, H.; He, Y.; Liao, B.-Q.; Lin, H., Thermodynamic analysis of effects of contact angle on interfacial interactions and its implications for membrane fouling control. *Bioresour. Technol.* **2016,** *201*, 245-252.

52. Bowen, W. R.; Hilal, N.; Lovitt, R. W.; Sharif, A. O.; Williams, P. M., Atomic force microscope studies of membranes: force measurement and imaging in electrolyte solutions. *J. Membr. Sci.* **1997,** *126*, (1), 77-89.

53. Brant, J. A.; Childress, A. E., Membrane–colloid interactions: comparison of extended DLVO predictions with AFM force measurements. *Environ. Eng. Sci.* **2002,** *19*, (6), 413-427.

54. Liu, G.; Li, L.; Qiu, L.; Yu, S.; Liu, P.; Zhu, Y.; Hu, J.; Liu, Z.; Zhao, D.; Yang, H.,

Chemical cleaning of ultrafiltration membranes for polymer-flooding wastewater treatment: Efficiency and molecular mechanisms. *J. Membr. Sci.* **2018,** *545*, 348-357.

55. Hong, S.; Elimelech, M., Chemical and physical aspects of natural organic matter (NOM) fouling of nanofiltration membranes. *J. Membr. Sci.* **1997,** *132*, (2), 159-181.

56. Lodhi, A.; Tahir, S.; Iqbal, Z.; Mahmood, A.; Akhtar, M.; Qureshi, T. M.; Yaqub, M.; Naeem, A., Characterization of commercial humic acid samples and their impact on growth of fungi and plants. *Soil and Environment* **2013,** *32*, 63-70.

57. Zydney, A. L.; Colton, C. K., A concentration polarization model for the filtrate flux in cross-flow microfiltration of particulate suspensions. *Chem. Eng. Commun.* **1986,** *47*, (1-3), 1-21.

58. Hoek, E. M. V.; Kim, A. S.; Elimelech, M., Influence of crossflow membrane filter geometry and shear rate on colloidal fouling in reverse osmosis and nanofiltration separations. *Environ. Eng. Sci.* **2002,** *19*, (6), 357-372.

59. Kim, S.; Hoek, E. M. V., Modeling concentration polarization in reverse osmosis processes. *Desalination* **2005,** *186*, (1-3), 111-128.

60. Wang, Y.-N.; Tang, C. Y., Fouling of nanofiltration, reverse osmosis, and ultrafiltration membranes by protein mixtures: the role of inter-foulant-species interaction. *Environ. Sci. Technol.* **2011,** *45*, (15), 6373-6379.

61. Goosen, M. F. A.; Sablani, S. S.; Ai-Hinai, H.; Ai-Obeidani, S.; Al-Belushi, R.; Jackson, D., Fouling of reverse osmosis and ultrafiltration membranes: A critical review. *Sep. Sci. Technol.* **2004,** *39*, (10), 2261-2297.

62. Tang, C. Y.; Kwon, Y.-N.; Leckie, J. O., Fouling of reverse osmosis and nanofiltration membranes by humic acid—Effects of solution composition and hydrodynamic conditions. *J. Membr. Sci.* **2007,** *290*, (1), 86-94.

63. Gao, W.; Liang, H.; Ma, J.; Han, M.; Chen, Z.-l.; Han, Z.-s.; Li, G.-b., Membrane fouling control in ultrafiltration technology for drinking water production: A review. *Desalination* **2011,** *272*, (1), 1-8.

64. Liu, J. X.; Tian, J.; Wang, Z. H.; Zhao, D. S.; Jia, F.; Dong, B. Z., Mechanism analysis of powdered activated carbon controlling microfiltration membrane fouling in surface water treatment. *Colloid Surface A* **2017,** *517*, 45-51.

65. Wang, Z.; Ma, J.; Tang, C. Y.; Kimura, K.; Wang, Q.; Han, X., Membrane cleaning in membrane bioreactors: a review. *J. Membr. Sci.* **2014,** *468*, 276-307.

66. Shi, X. F.; Tal, G.; Hankins, N. P.; Gitis, V., Fouling and cleaning of ultrafiltration membranes: A review. *J. Water Process Eng.* **2014,** *1*, 121-138.